ACS PHYSICAL CHEMISTRY Au
AN OPEN ACCESS JOURNAL OF THE AMERICAN CHEMICAL SOCIETY



pubs.acs.org/physchemau
Article

# Design Criteria for Active and Selective Catalysts in the Nitrogen Oxidation Reaction

Muhammad Usama,[‖] Samad Razzaq,[‖] and Kai S. Exner*

Cite This: ACS Phys. Chem Au 2025, 5, 38−46
Read Online
ACCESS | Metrics & More | Article Recommendations | Supporting Information

**ABSTRACT:** The direct conversion of dinitrogen to nitrate is a dream reaction to combine the Haber−Bosch and Ostwald processes as well as steam reforming using electrochemistry in a single process. Regrettably, the corresponding nitrogen oxidation (NOR) reaction is hampered by a selectivity problem, since the oxygen evolution reaction (OER) is both thermodynamically and kinetically favored in the same potential range. This opens the search for the identification of active and selective NOR catalysts to enable nitrate production under anodic reaction conditions. While theoretical considerations using the computational hydrogen electrode approach have helped in identifying potential material motifs for electrocatalytic reactions over the last decades, the inherent complexity of the NOR, which consists of ten proton-coupled electron transfer steps and thus at least nine intermediate states, poses a challenge for electronic structure theory calculations in the realm of materials screening. To this end, we present a different strategy to capture the competing NOR and OER at the atomic scale. Using a data-driven method, we provide a framework to derive generalized design criteria for materials with selectivity toward NOR. This leads to a significant reduction of the computational costs, since only two free-energy changes need to be evaluated to draw a first conclusion on NOR selectivity.

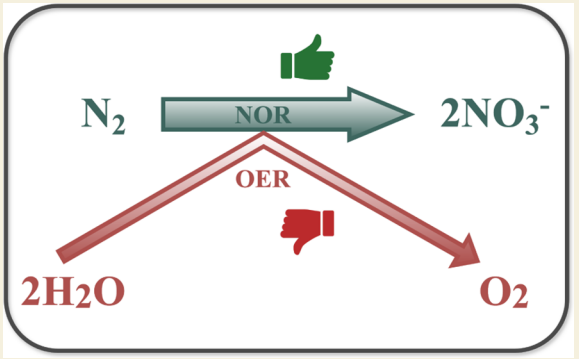


**KEYWORDS:** *nitrogen oxidation reaction, oxygen evolution reaction, descriptor approach, scaling relation, selectivity*

## 1. INTRODUCTION

Dinitrogen ($N_2$) is the largest single component of the Earth's atmosphere (around 78% by volume). While $N_2$ is inert under mild conditions due to its strong N≡N triple bond, fixation of $N_2$ is essential for life on earth, and the cleavage of the N≡N triple bond to form valuable nitrogen-based compounds is an ongoing challenge.[1,2]

The most important nitrogen commodity is ammonia ($NH_3$), with an annual production of more than 150 million metric tons.[3] Direct reduction of dinitrogen to ammonia is traditionally carried out by the Haber-Bosch process, using metal-based catalysts of group VIII (Fe, Ni, Ru, Pt, among others) at elevated temperatures and pressures to allow for ammonia formation at reasonable rates.[4] Although the Haber−Bosch process is one of the most influential inventions of the 20th century and has led to a global population of more than 8.1 billion people today, it is energy intensive and has a significant carbon footprint since the required gaseous hydrogen is mainly produced by steam reforming methane.[5]

While it appears to be a formidable task, it is yet highly desirable to replace the Haber-Bosch process by environmentally friendly routes to mitigate the emission of greenhouse gases.[6] A promising starting point refers to electrochemical nitrogen reduction (NRR) for ammonia formation.[7−9] Yet, this process is still in its infancy due to the low solubility of $N_2$ in water, the competition with the hydrogen evolution reaction (HER) under cathodic reaction conditions, and the slow reaction kinetics due to the transfer of six proton−electron pairs to form $NH_3$.[10] Faradaic efficiencies for the formation of ammonia are commonly far below 50% in aqueous media, and the reported values even need to be treated with caution because only the usage of $^{15}N$ isotope labeling experiments allows rendering reliable conclusions on ammonia selectivity.[11]

The majority of ammonia from the Haber-Bosch process enters the Ostwald process to produce nitric acid ($HNO_3$), which is the second most important nitrogen commodity with an annual production of about 50 million metric tons.[3] Consequently, nearly all $HNO_3$ is manufactured by a three-stage approach by combining steam reforming methane with the Haber-Bosch and Ostwald processes.[12] This is an energetically unfavorable scenario, which could be readily improved by making use of electrochemistry,[13,14] such as by directly converting dinitrogen from the air into $HNO_3$ or

Received: July 18, 2024
Revised: December 7, 2024
Accepted: December 9, 2024
Published: December 24, 2024

nitrate ($NO_3^-$). The direct conversion of dinitrogen to nitrate by the nitrogen oxidation reaction (NOR; cf. eq 1) is also preferred over the coupling of the electrochemical analogues of the Haber–Bosch and Ostwald processes, i.e., the NRR and ammonia oxidation reactions (AOR), which require cathodic or anodic reaction conditions, respectively (cf. Figure 1).

$$N_2 + 6H_2O \rightarrow 2NO_3^- + 12H^+ + 10e^-,$$
$$U^0_{NOR} = 1.25\ \text{V vs. RHE (reversible hydrogen electrode)}$$
$$@\text{pH} = 0 \quad (1)$$

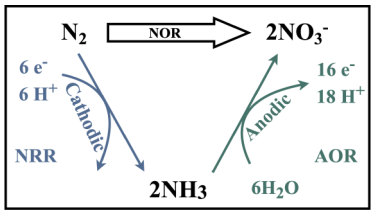


**Figure 1.** Electrochemical nitrogen cycle consisting of dinitrogen ($N_2$), ammonia ($NH_3$), and nitrate ($NO_3^-$). While electrochemical analogues to the Haber–Bosch and Ostwald processes for the formation of $NH_3$ and $NO_3^-$ refer to the nitrogen reduction (NRR) and ammonia oxidation (AOR) reactions, respectively, the direct electrochemical oxidation of $N_2$ to $NO_3^-$ is a dream reaction for which selective electrocatalysts have yet to be found.

We note that the equilibrium potential of the NOR is pH dependent on the RHE scale due to the different number of protons and electrons in the above reaction equation:[15] at pH = 14, $U^0_{NOR}$ is reduced to 1.08 V vs RHE. It should also be considered that, besides nitrate, other oxidized nitrogen species such as NO, $N_2O$, or $NO_2^-$ can be formed under anodic reaction conditions. However, their equilibrium potentials exceed $U^0_{NOR}$ by several hundred millivolts, and this is the reason why we focus our analysis on the thermodynamically favored product–nitrate.

Without any ado, the NOR offers attractive advantages over the conventional three-stage approach in that the formation of nitric acid can be carried out at room temperature rather than at elevated temperatures, and the required electricity can be taken from renewable energy sources, making the process sustainable.[16,17] Similar to the NRR in aqueous media, the development of active, stable, and selective NOR catalysts is still in its infancy.[18−21] Unfortunately, the oxygen evolution reaction (OER) represents a detrimental side reaction in the same potential window (cf. eq 2), limiting the Faraday efficiency of forming valuable nitrogen compounds:

$$2H_2O \rightarrow O_2 + 4H^+ + 4e^-, \quad U^0_{OER} = 1.23\ \text{V vs. RHE} \quad (2)$$

The selectivity challenge between the NOR and OER is even more pronounced than in other anodic processes (e.g., competition between the chlorine evolution and oxygen evolution reactions in a chloride-containing electrolyte)[22] as the OER is both thermodynamically (lower equilibrium potential) and kinetically (less electrons transferred) preferred over the NOR. This makes the development of selective NOR catalysts challenging and rewarding at the same time. So far, there are only a few experimental reports on Pd-based materials that allow for the formation of nitrogen compounds with moderate Faraday efficiencies under the harsh anodic reaction conditions.[23,24]

Since the birth of the computational hydrogen electrode (CHE) approach at the beginning of the 21st century,[25] electronic structure calculations in the density functional theory (DFT) approximation have been thought to enable the identification of active and selective material motifs for electrocatalytic processes. While the evaluation of adsorption free energies analyzed by means of heuristic descriptor has proven successful for the two-electron hydrogen evolution reaction or the OER,[26−28] determining the full NOR free-energy landscape is challenging due to the increasing number of intermediate states in the catalytic cycle.[29] To this end, previous theoretical works using DFT relied on a different strategy as the entire NOR pathway leading to nitrate formation (cf. eq 1) was not modeled, but rather the partial oxidation of dinitrogen to $N_2O$ or NO was investigated.[12,30−33] Given that the equilibrium potentials for the electrochemical transformation of $N_2$ into $N_2O$, NO, $NO_2^-$, or $NO_3^-$ are all different, it cannot be concluded that a catalyst with selectivity toward $N_2O$, NO, or $NO_2^-$ formation is equally selective for the electrochemical synthesis of $NO_3^-$.[34]

The present manuscript fills this gap by investigating the competition between nitrate and oxygen formation at the atomic level (cf. eqs 1 and 2). Instead of applying DFT calculations[35,36] for a selected material, we are interested in general trends and design criteria for selective NOR culminating in the formation of $NO_3^-$. Therefore, we make use of a data-driven strategy by analyzing adsorption free energies using the descriptor $G_{max}(U)$,[37,38] which has been proven successful in previous studies on the OER, NRR, or oxygen reduction reaction.[39−41] In contrast to these previous studies, we additionally focus on the competition of these competing reaction channels at different pH values, studying both acidic (pH = 0) and alkaline (pH = 14) conditions. Our methodology enables the derivation of benchmarks for active and selective electrocatalysis, which can be used in future DFT-based work via high-throughput screening of NOR catalysts to accelerate the identification of promising material motifs for the formation of $NO_3^-$ under applied bias.

## 2. METHODS

We use an in-house approach in which we define the reaction channels under consideration (OER and NOR) by a "basis set" of adsorption free energies. A detailed discussion of this methodology can be found in the literature where our methodology was recently reviewed.[42]

### 2.1. Oxygen Evolution Reaction (OER)

OER is considered to proceed through four proton-coupled electron transfer steps, with subsequent formation of the *OH, *O, and *OOH adsorbates on the catalytically active center[43] (*):

$$^* + H_2O \rightarrow {}^*OH + H^+ + e^- \quad \Delta G_1 \quad (3)$$
$$^*OH \rightarrow {}^*O + H^+ + e^- \quad \Delta G_2 \quad (4)$$
$$^*O + H_2O \rightarrow {}^*OOH + H^+ + e^- \quad \Delta G_3 \quad (5)$$
$$^*OOH \rightarrow {}^* + O_2 + H^+ + e^- \quad \Delta G_4 \quad (6)$$

While our recent works highlighted that the mechanistic diversity in the OER has been largely overlooked in previous DFT-based studies,[44] we restrict the analysis of the OER to the mononuclear mechanism (cf. eqs 3–6) because we are essentially interested in


https://doi.org/10.1021/acsphyschemau.4c00058
ACS Phys. Chem Au 2025, 5, 38−46

qualitative trends between the NOR and OER and not in the identification of highly active OER catalysts. For this purpose, considering a single mechanistic pathway for the OER is sufficient.[45,46]

It is important to note that the binding energies of the *OH, *O, and *OOH intermediates are intrinsically coupled due to the presence of scaling relations between these adsorbate species.[45] The correlation between the *OH and *OOH intermediates is strong regardless of the material class, and the corresponding scaling relationship reads (cf. eq 7):

$$\Delta G_2 + \Delta G_3 = (3.20 \pm 0.20)\ \text{eV} \tag{7}$$

Note that in our analysis, we have also considered values of 3.00 and 2.80 eV in addition to a scaling-relation intercept of 3.20 eV.[47,48] Further information is provided in Section S1.

A different situation is encountered with the scaling relation between the *OH and *O intermediates.[49] This correlation is less pronounced, which may be related to the different bond orders of the *O intermediate at dissimilar active sites (single bonds vs. double bond[50]). While various scaling relationships for the *OH vs. *O scaling relation, considering or neglecting a scaling-relation intercept, can be found in the literature,[51−55] we use the description in eq 8 in accordance with previous works:[40,44]

$$\Delta G_2 = 2\cdot\Delta G_1 \tag{8}$$

Application of this scaling relation allows gaining insight into general trends of the OER in dependence of the free-energy change $\Delta G_1$, which is related to the formation of the *OH intermediate (cf. eq 3). Note that $\Delta G_1$ is the only free variable for the mechanistic description of eqs 3−6, as the free-energy change $\Delta G_4$ is governed by the equilibrium potential of the OER using the concept of gas-phase error corrections[56,57] (cf. eqs 9 and 10):

$$\Delta G_1 + \Delta G_2 + \Delta G_3 + \Delta G_4 = 4\cdot e\cdot U^0_{\text{OER}} = 4.92\ \text{eV} \tag{9}$$

$$\Delta G_4 = 4.92\ \text{eV} - (\Delta G_1 + \Delta G_2 + \Delta G_3) = 1.72\ \text{eV} - \Delta G_1 \tag{10}$$

To this end, we use a basis set for the free variable $\Delta G_1$, which reads:

$$\Delta G_1 = [-0.5,\ 2.2;\ 0.3]\ \text{eV} \tag{11}$$

In eq 11, the first two values in the rectangular brackets indicate the start and stop values, whereas the value following ";" denotes the step size between any two consecutive values. The choice of this data set for $\Delta G_1$ ultimately refers to the data collection of Divanis et al. on metallic and semiconducting oxides from a decade of atomic scale simulations.[51] Note that the large step size of 0.3 eV compared to previous works on the OER is related to a reduction of the overall amount of data due to the considerable data size for the description of the NOR (*vide infra*). In Section S1, we have benchmarked the application of the reduced data set for describing the OER by a volcano plot (cf. Figure S4).

Knowledge of the free-energy changes $\Delta G_n$ ($n$ = 1, 2, 3, 4) makes it possible to express the free energies of the intermediate states in the catalytic cycle of eqs 3−6 as a function of $\Delta G_1$:[44]

$$G(^*) = 0\ \text{eV} \tag{12}$$

$$G(^*\text{OH}) = \Delta G_1 - 1\cdot e\cdot U \tag{13}$$

$$G(^*\text{O}) = \Delta G_1 + \Delta G_2 - 2\cdot e\cdot U = 3\cdot\Delta G_1 - 2\cdot e\cdot U \tag{14}$$

$$G(^*\text{OOH}) = \Delta G_1 + \Delta G_2 + \Delta G_3 - 3\cdot e\cdot U = \Delta G_1 + 3.20\ \text{eV} - 3\cdot e\cdot U \tag{15}$$

$$G(^* + \text{O}_2) = \Delta G_1 + \Delta G_2 + \Delta G_3 + \Delta G_4 - 4\cdot e\cdot U = 4.92\ \text{eV} - 4\cdot e\cdot U \tag{16}$$

Note that the CHE approach[25] is used to describe the potential dependence in eqs 12−16.

The free energies of the reaction intermediates are analyzed by the descriptor $G_{\text{max}}(U)$, which is a potential-dependent activity measure based on the concept of the free-energy span model.[37,38] While the conventionally applied activity descriptor − the thermodynamic overpotential[58] − approximates the electrocatalytic activity based on a single free-energy change at the equilibrium potential of the OER, $G_{\text{max}}(U)$ analyzes all possible free-energy spans between the intermediate states in a potential-dependent fashion. The largest free-energy span is a measure for the electrocatalytic activity because it has been demonstrated in previous work that $G_{\text{max}}(U)$ directly scales with the electrocatalytic activity due to a potential-dependent Brønsted−Evans−Polanyi (BEP) relation.[37] Equation 17 illustrates the procedure to determine the descriptor $G_{\text{max}}(U)$ for the OER:

$$\begin{aligned} G^{\text{OER}}_{\text{max}}(U) = \max\{&G(^*\text{OH}) - G(^*);\ G(^*\text{O}) - G(^*);\ G(^*\text{OOH}) - G(^*);\\ &G(^*\text{O}) - G(^*\text{OH});\ G(^*\text{OOH}) - G(^*\text{OH});\\ &G(^* + \text{O}_2) - G(^*\text{OH});\ G(^*\text{OOH}) - G(^*\text{O});\\ &G(^* + \text{O}_2) - G(^*\text{O});\ G(^* + \text{O}_2) - G(^*\text{OOH})\} \end{aligned} \tag{17}$$

Note that in contrast to the thermodynamic overpotential, the limiting free-energy span can change when the applied electrode potential is varied. Such an alteration in the limiting free-energy span can be related to a change in the rate-determining step, which is experimentally visible by a switch in the Tafel slope.[59] To this end, the descriptor $G_{\text{max}}(U)$ captures overpotential and kinetic effects in the assessment of the electrocatalytic activity while relying on the analysis of adsorption free energies. For further information on the descriptor $G_{\text{max}}(U)$, we refer to the current literature.[38]

We choose three different applied electrode potentials to evaluate the electrocatalytic activity in the OER using the descriptor $G^{\text{OER}}_{\text{max}}(U)$, namely $U$ = [1.40, 1.50, 1.60] V vs RHE. At all three potentials, we construct a volcano plot by plotting $G^{\text{OER}}_{\text{max}}(U)$ as a function of $\Delta G_1$, which is shown in Figures S1−S3 (cf. Section S1). This procedure is necessary to assess the selectivity for nitrate formation at a later stage by comparing the descriptors $G^{\text{OER}}_{\text{max}}(U)$ and $G^{\text{NOR}}_{\text{max}}(U)$.

## 2.2. Nitrogen Oxidation Reaction (NOR)

NOR is a complex process in which 10 electrons are transferred when a single molecule of dinitrogen is converted into two molecules of nitric acid or nitrate. Since the electron transfer occurs sequentially, at least nine intermediate states are conceivable during the catalytic cycle. In addition, the recent work by Nørskov and coworkers on the NOR indicated that surface *OH is necessary to activate the dinitrogen molecule.[12] Therefore, we suggest the following pathway for the conversion of $N_2$ into nitric acid:

$$^* + \text{H}_2\text{O} \rightarrow {}^*\text{OH} + \text{H}^+ + \text{e}^- \quad \Delta G_1 \tag{18}$$

$$^*\text{OH} + \text{N}_2 \rightarrow {}^*\text{N}_2\text{OH} \quad \Delta G_a \tag{19}$$

$$^*\text{N}_2\text{OH} \rightarrow {}^*\text{N}_2\text{O} + \text{H}^+ + \text{e}^- \quad \Delta G_b \tag{20}$$

$$^*\text{N}_2\text{O} + \text{H}_2\text{O} \rightarrow {}^*\text{N}_2\text{O}_2\text{H} + \text{H}^+ + \text{e}^- \quad \Delta G_c \tag{21}$$

$$^*\text{N}_2\text{O}_2\text{H} \rightarrow {}^*\text{N}_2\text{O}_2 + \text{H}^+ + \text{e}^- \quad \Delta G_d \tag{22}$$

$$^*\text{N}_2\text{O}_2 + \text{H}_2\text{O} \rightarrow {}^*\text{NO}_2\text{H} + {}^*\text{NO} + \text{H}^+ + \text{e}^- \quad \Delta G_e \tag{23}$$

$$^*\text{NO}_2\text{H} + {}^*\text{NO} + \text{H}_2\text{O} \rightarrow {}^*\text{NO}_2\text{H} + {}^*\text{NO}_2\text{H} + \text{H}^+ + \text{e}^- \quad \Delta G_f \tag{24}$$

$$^*\text{NO}_2\text{H} + {}^*\text{NO}_2\text{H} \rightarrow {}^*\text{NO}_2 + {}^*\text{NO}_2\text{H} + \text{H}^+ + \text{e}^- \quad \Delta G_g \tag{25}$$



https://doi.org/10.1021/acsphyschemau.4c00058
ACS Phys. Chem Au 2025, 5, 38−46

$$^{*}NO_2 + {}^{*}NO_2H \rightarrow {}^{*}NO_2 + {}^{*}NO_2 + H^+ + e^- \quad \Delta G_h \tag{26}$$

$$^{*}NO_2 + {}^{*}NO_2 + H_2O \rightarrow {}^{*}NO_3H + {}^{*}NO_2 + H^+ + e^- \quad \Delta G_i \tag{27}$$

$$^{*}NO_3H + {}^{*}NO_2 + H_2O \rightarrow {}^{*}NO_3H + {}^{*}NO_3H + H^+ + e^- \quad \Delta G_j \tag{28}$$

$$^{*}NO_3H + {}^{*}NO_3H \rightarrow 2^{*} + 2NO_3H \quad \Delta G_k \tag{29}$$

Similar to the OER, we set up a "basis set" for the elementary reaction steps of the NOR. However, the situation is fundamentally different here, as only a few DFT-based studies on the NOR are available in the literature.[12,30−33] Regrettably, these works do not report scaling relations for the nitrogen intermediates of eqs 18−29 and consequently, we define a basis set for the free-energy changes as follows:

$$\Delta G_1 = [-0.5,\ 2.2;\ 0.3]\ \text{eV} \tag{30}$$

$$\Delta G_n = [-3.0,\ 3.0;\ 1.\ 0]\ \text{eV for}\ n = \{a, b, c, ..., j\} \tag{31}$$

Note that eq 31 is a generalized expression for the data range of free-energy changes with respect to the nitrogen intermediates. We emphasize that the presented approach is agnostic to the exact chemical nature of the proposed mechanism (cf. eqs 18−29), and the only relevant information extracted from it is the number of chemical or electrochemical steps. This information is already sufficient to describe the selectivity of the NOR and OER, as explained in more detail below.

Note that scaling relations between the intermediate states are expected since it was demonstrated in previous works that there is a correlation between the adsorption free energies of nitrogen intermediates in the NRR. We infer that knowledge of the unknown scaling relations between the NOR intermediates would reduce the data range of eq 31 to a subset. Therefore, our approach can be interpreted as an "upper bound analysis" by analyzing a larger parameter space for the free-energy changes of $\Delta G_n$ as available in a class of materials. However, this train of thought already allows us to derive general trends in NOR selectivity. In addition, our data-driven model of eqs 18−31 could be refined at a later stage once scaling relationships for the intermediate states have been calculated by DFT in a homologous series of materials (*vide infra*). Last but not least, since we assume a generalized basis set to capture trends in the NOR, our data-driven study is not strictly dependent on the chosen mechanistic description (cf. eqs 18−29). Similar expressions can also be derived for other pathways leading to nitrate formation, thus making our model universal to capture essential features of selective NOR at the atomic level.

In Section S2, we provide a detailed derivation of the free energies of the intermediate states and the descriptor $G_{max}^{NOR}(U)$ in the NOR (cf. eqs S28−S42). As with the OER, we assess the energetics at three different applied electrode potentials, namely $U = [1.40, 1.50, 1.60]$ V vs RHE. This allows us to render potential-dependent conclusions on the NOR activity and selectivity by integrating the data pairs $(\Delta G_1; G_{max}^{NOR}(U))$ into the OER volcano plot. Note that the difference between $G_{max}^{OER}(U)$ and $G_{max}^{NOR}(U)$ is a measure for NOR selectivity:

$$G_{sel}(U) = G_{max}^{OER}(U) - G_{max}^{NOR}(U) \tag{32}$$

Based on $G_{sel}(U)$, we can express the NOR selectivity in percent:[60]

$$\text{NOR selectivity}\ (U) = \exp(G_{sel}(U)/k_BT)/[\exp(G_{sel}(U)/k_BT) + 1] \tag{33}$$

In eq 33, $k_B$ and $T$ indicate Boltzmann's constant and absolute temperature in Kelvin, respectively.

We emphasize that the low solubility of $N_2$ in aqueous electrolytes can be a limiting factor for the NOR.[23,61] In Section S5, we discuss our model assumption on how the $N_2$ concentration in the Helmholtz layer can affect the predicted NOR selectivity (cf. eq 33). In addition, we provide a pH-dependent analysis of NOR selectivity in Section S6.

The above-introduced data-driven framework is executed for the basis set defined used to describe the OER and NOR (cf. eqs 9−11 and 30 and 31). This results in a total of 28,343,520 data points for the three different applied electrode potentials or 9,447,840 data points per $U$-value. We can relate this to the fact that we have considered 9,447,840 different catalysts in our data-driven study, as each data points corresponds to a different material. The only downside to analyzing this huge amount of data is that at this point, we do not know which data point belongs to which material. In addition, we do not know if all these materials can be synthesized, as some of them may not satisfy the currently unknown scaling relationships between the NOR intermediates. Nevertheless, our data-driven investigation provides unprecedented insights into controlling selectivity toward nitrate formation and deriving design criteria for selective NOR by considering the complete conversion of dinitrogen to nitrate, which is further discussed in the following section.

## 3. RESULTS AND DISCUSSION

Using our in-house Python code (cf. Section S4) to evaluate the selectivity challenge between nitrate and oxygen formation, we analyze the NOR selectivity (cf. eq 33) at pH = 0 for all 28,343,520 data points. Tables 1 provides a statistical overview.

**Table 1. Statistical Analysis of the Nitrogen Oxidation and Oxygen Evolution Reactions for the Considered Dataset of 28,343,520 Data Points at pH = 0[a]**

| NOR Selectivity | Number of Cases | Percentage of Cases |
|---|---|---|
| 0 | 27,102,376 | 95.62 |
| 0.02 | 67,323 | 0.24 |
| 0.04 | 15,965 | 0.06 |
| 0.5 | 22,308 | 0.08 |
| 0.69 | 32,461 | 0.11 |
| 0.98 | 81,304 | 0.29 |
| 0.99 | 10,619 | 0.04 |
| 1 | 10,111,64 | 3.57 |

[a]NOR selectivity is determined according to eq 33.

Table 1 reveals that only discrete values for the NOR selectivity are observed. Note that there are two reasons for this finding: on the one hand, we have used a discrete rather than continuous representation of the OER and NOR basis sets (cf. eqs 9−11 and 30 and 31). On the other hand, the evaluation of the NOR selectivity based on eq 33 leads to discrete values due to the presence of exponential terms in the numerator and denominator. To this end, we do not aim to interpret the selectivity values quantitatively, but rather strive for a qualitative assessment. Without any ado, our main interest refers to data points with high NOR selectivity, and thus we further analyze the distribution for NOR selectivity ≥0.98. Altogether, 11,030,87 data points meet this criterion, which is only about 3.90% of our entire data set. On the contrary, about 95.86% of all data points (27,169,699 out of 28,343,520) show distinct selectivity toward the OER (NOR selectivity ≤0.02). This outcome could have been expected based on the thermodynamic and kinetic comparison of the NOR and OER (cf. eqs 1 and 2), indicating that the identification of highly selective NOR catalysts is challenging. To further scrutinize the factors that govern selective nitrate formation, we analyze the impact of the applied electrode potential on the NOR selectivity. Figure 2 provides a potential-dependent evaluation of the NOR selectivity for data points


https://doi.org/10.1021/acsphyschemau.4c00058
ACS Phys. Chem Au 2025, 5, 38−46

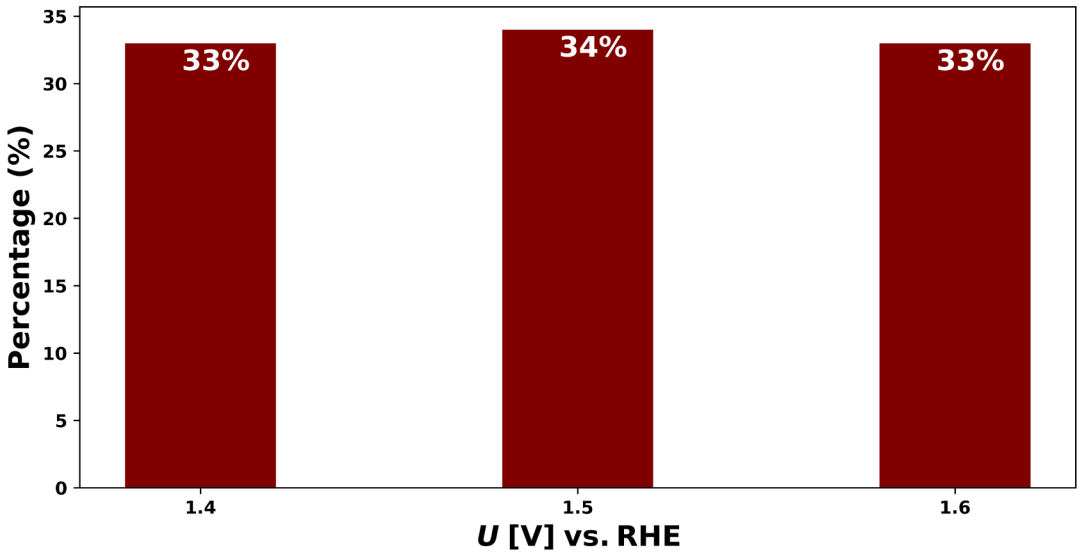


**Figure 2.** Potential-dependent evaluation of the NOR selectivity at $U = [1.40, 1.50, 1.60]$ V vs RHE and pH = 0 for all data points where at least 98% selectivity for nitrate is observed.

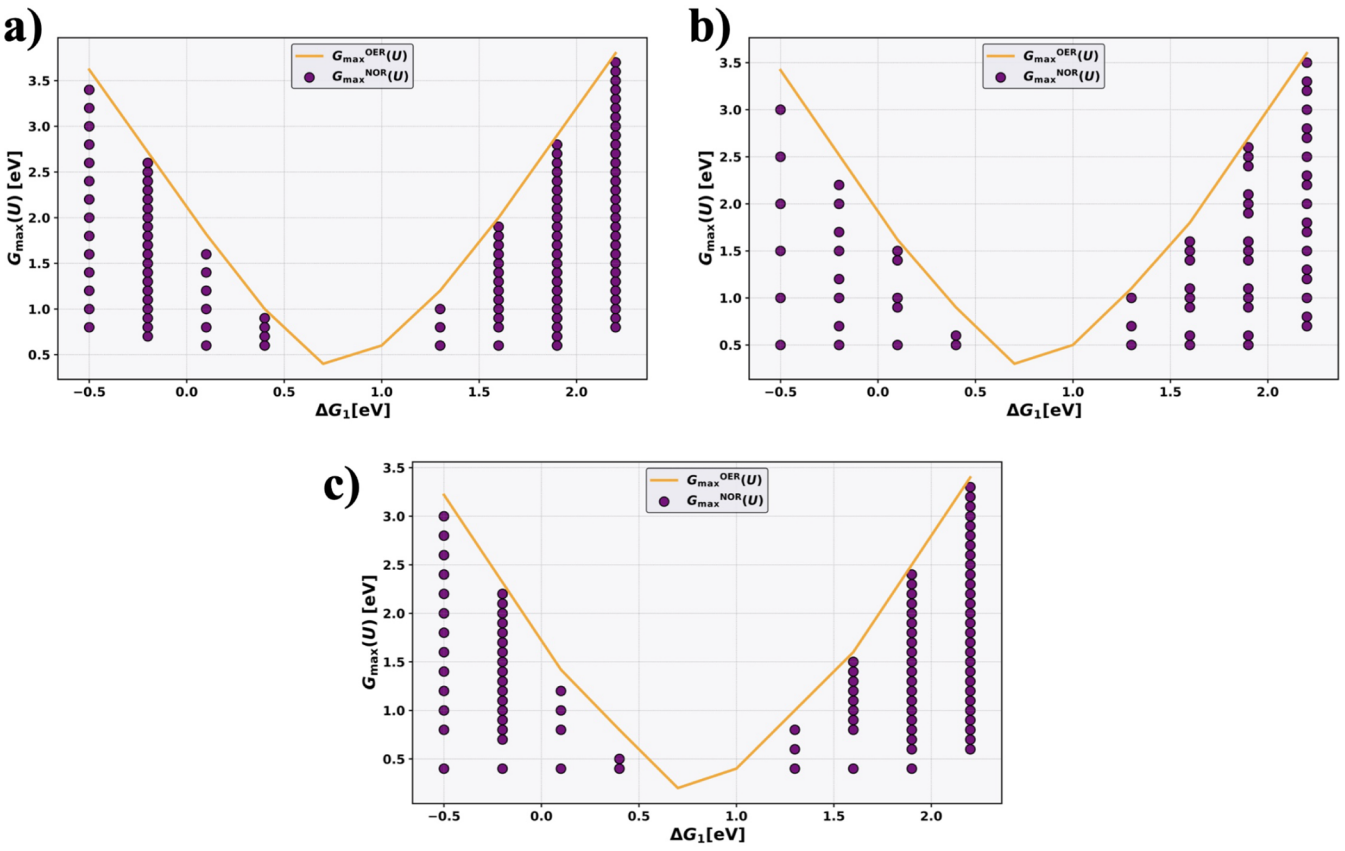


**Figure 3.** Volcano plot for the oxygen evolution reaction (OER in yellow) and data points for the nitrogen oxidation reaction (NOR in maroon) with NOR selectivity ≥0.98 at pH = 0 for (a) $U$ = 1.40 V vs RHE, (b) $U$ = 1.50 V vs RHE, and (c) $U$ = 1.60 V vs RHE.

that satisfy the precondition of NOR selectivity ≥0.98. We observe no clear potential dependence of the NOR selectivity in the considered potential range of 1.40−1.60 V vs RHE. This finding is in qualitative agreement with experimental studies on Pd-based materials in the same potential range.[24]

To comprehend general trends in the NOR selectivity, we adopt the OER volcano plot (cf. Figure S1) and add the data points that fulfill the requirement of NOR selectivity ≥0.98. This enables discussing NOR selectivity by using the adsorption free energy of the *OH intermediate − $\Delta G_1$ (cf. eqs 3 and 18) − as a descriptor, as illustrated in Figure 3.

The potential-dependent evaluation of the volcano plot shows a consistent picture for selective NOR: all data points fulfilling NOR selectivity ≥0.98 are located at the left − $\Delta G_1$ < 0.50 eV − or right − $\Delta G_1$ > 1.20 eV − legs (low OER activity) rather than at the apex (high OER activity) of the volcano plot.


https://doi.org/10.1021/acsphyschemau.4c00058
ACS Phys. Chem Au 2025, 5, 38−46

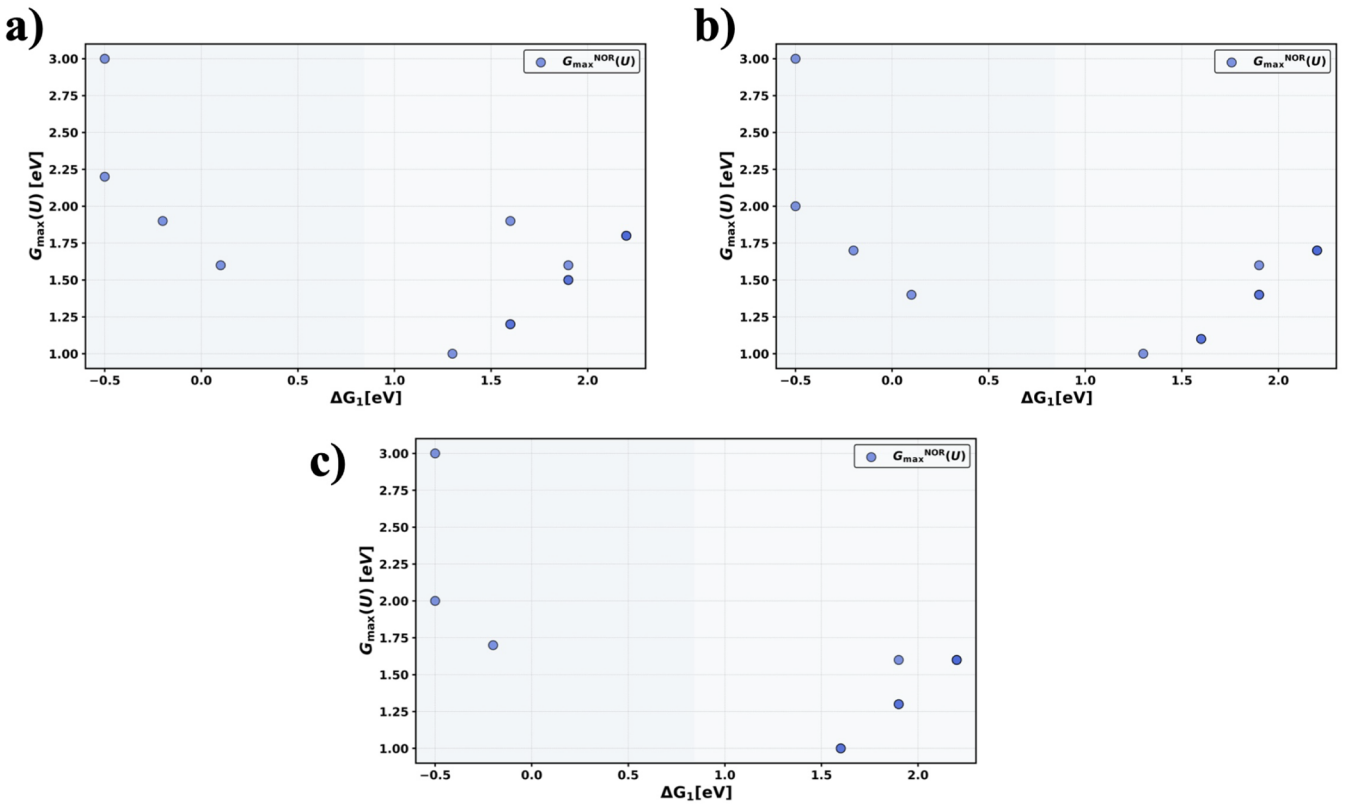


**Figure 4.** Activity plot for the nitrogen oxidation reaction (NOR) with NOR selectivity ≥0.98 at pH = 0 for (a) $U$ = 1.40 V vs RHE, (b) $U$ = 1.50 V vs RHE, and (c) $U$ = 1.60 V vs RHE.

This finding underpins that state-of-the-art OER electrocatalysts, such as transition-metal oxides in the form of $IrO_2$ or NiFeOOH,[62,63] are not potential candidate materials for selective NOR. Consequently, this outcome allows us to reduce the search of promising material motifs for the NOR to inactive OER catalysts. It is noteworthy that already the calculation of a single adsorption free energy, namely $\Delta G_1$, enables assessing the suitability of a particular catalytic site for the OER based on the location in the volcano plot (cf. Figure 3). Therefore, we have successfully identified a first criterion for the high-throughput screening of material motifs for the NOR based on the evaluation of $\Delta G_1$.

Although selectivity is a more pressing issue than the activity of NOR catalysts, we further consider the evaluation of the electrocatalytic NOR activity based on the descriptor $G_{max}^{NOR}(U)$. Figure 4 shows the respective data points that fulfill the requirement of NOR selectivity ≥0.98 in dependence of $\Delta G_1$ in the potential range of 1.40−1.60 V vs RHE. While Figure 4 relies on the adoption of a scaling-relation intercept of 3.20 eV for the *OH and *OOH intermediates (cf. eq 7), we provide the same analysis for the corresponding values of 3.00 and 2.80 eV in Section S3 (cf. Figures S5−S7).

Figure 4 illustrates that there is a stark difference in the electrocatalytic activity for the NOR at the left ($\Delta G_1$ < 0.50 eV) and right ($\Delta G_1$ > 1.20 eV) volcano legs. While the activity is small at the left leg as $G_{max}^{NOR}(U)$ exceeds 2.00 eV, a different situation arises for $\Delta G_1$ > 1.20 eV, where high activity is observed due to a significantly reduced value of $G_{max}^{NOR}(U)$. We relate this difference in the electrocatalytic activity in dependence of the binding energy of *OH ($\Delta G_1$) to different adsorbate coverages under reaction conditions. For strong oxygen binding ($\Delta G_1$ < 0.50 eV), a high *OH/*O coverage is expected under the anodic reaction conditions, which impedes the adsorption of the reactant $N_2$ for the NOR. In contrast, for weak oxygen binding ($\Delta G_1$ > 1.20 eV), a smaller *OH/*O coverage provides sufficient vacancies for the adsorption of $N_2$, which facilitates the interaction of $N_2$ and *OH to activate dinitrogen for conversion to nitrate. To this end, it is expedient to restrict the search of potential candidate materials for the NOR to the right volcano leg ($\Delta G_1$ > 1.20 eV), since only weak oxygen binding provides access to material motifs with reasonable activity in the NOR. Given that also the adsorption of $N_2$ (cf. eq 19) must not be thermodynamically unfavorable for dinitrogen conversion (i.e., $\Delta G_a$ < 0.50 eV[64]), we propose the conjoint assessment of $\Delta G_1$ and $\Delta G_a$ to accelerate the identification of promising materials motifs for the NOR based on high-throughput screening using DFT calculations combined with artificial intelligence and machine learning techniques.[65,66] This suggestion also applies to the assessment of the NOR under alkaline conditions, as further discussed in Section S6.

While the present manuscript does not aim to propose novel catalytic materials for the NOR, but rather to accelerate the discovery of these electrocatalysts by deriving simple descriptors, we emphasize that our data-driven model can be further used after performing comprehensive DFT calculations through a feedback loop. As soon as information on the scaling between the nitrogen intermediates in the NOR following the generalized scheme of eqs 18−29 is available, it allows to refine the basis set of eq 31 for the description of the NOR pathways and to reduce our current "upper bound analysis" to the available material space. Figure 5 summarizes the discussion on this line of thought.


https://doi.org/10.1021/acsphyschemau.4c00058
ACS Phys. Chem Au 2025, 5, 38−46

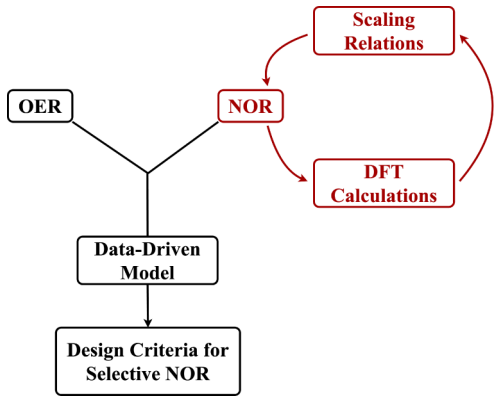


**Figure 5.** Feedback loop to support the derivation of design criteria for selective nitrogen-oxidation reaction (NOR) catalysts. Our generalized approach to the NOR (cf. Section S4) can be refined by applying DFT calculations to determine scaling relations in a class of materials. If this knowledge is incorporated into the description of the NOR (cf. eqs 18−33), it could provide insight beyond the proposed conditions of $\Delta G_1 > 1.20$ eV and $\Delta G_a < 0.50$ eV that apply to any active and selective NOR catalyst.

Finally, we point out that the selectivity problem between the competing NOR and OER is even more complex, since the gaseous $O_2$ formed in the OER can serve as an oxidant for $N_2$ at the solid/liquid interface. Therefore, the harmful OER could also have a positive effect by opening new reaction channels for the activation of the inert dinitrogen molecule. In the present manuscript, however, we rely on the discussion of decoupled pathways in the context of the NOR and OER (cf. eqs 3−29). It is recommended that future studies using DFT should inspect the impact of $N_2$ activation as a function of both the electrochemical environment and $p(O_2)$ as a result of the ongoing OER as a side reaction.

## 4. CONCLUSIONS

Direct conversion of dinitrogen from the air into nitric acid is a dream reaction that can be achieved using electrochemistry (cf. Figure 1) if selective catalysts for the nitrogen oxidation reaction (NOR) are developed. While theoretical studies to predict candidate materials that are later tested experimentally have gained unprecedented popularity in recent decades, a thorough investigation of the elementary steps in the NOR is challenging due to the significant number of proton-coupled electron transfers in the reaction mechanism (cf. eqs 18−29). To overcome this challenge, we have developed a pH-dependent data-driven assessment based on the construction of volcano plots to identify design criteria for active and selective NOR catalysts in acid and base, considering that the oxygen evolution reaction (OER) is a detrimental side reaction in the same potential window that is thermodynamically and kinetically favored over the NOR.

Our pH-dependent evaluation shows that the chances of identifying selective materials for the NOR are modest overall (cf. Table 1), and the NOR selectivity is not largely potential dependent (cf. Figure 2). Using the concept of volcano-based selectivity and activity plots (cf. Figures 3 and 4), we propose the conjoint assessment of $\Delta G_1 > 1.20$ eV and $\Delta G_a < 0.50$ eV (cf. eqs 18 and 19) in theoretical studies using electronic structure theory to enable high-throughput screening of potential candidate materials. We strongly recommend that future studies derive scaling relationships of NOR intermediates using electronic structure theory, as this knowledge for a class of materials can be integrated into our generalized data-driven model through a feedback loop (cf. Figure 5). This strategy may pave the way for the derivation of descriptors beyond the proposed assessment of $\Delta G_1$ and $\Delta G_a$ as well as for the identification of material motifs for selective NOR.

## ■ ASSOCIATED CONTENT

### Supporting Information

The Supporting Information is available free of charge at https://pubs.acs.org/doi/10.1021/acsphyschemau.4c00058.

Theoretical description of the oxygen evolution reaction; theoretical description of the nitrogen oxidation reaction; activity plots for the nitrogen oxidation reaction; pseudocode for the data-driven analysis of the nitrogen oxidation and oxygen evolution reactions; model assumption for $N_2$ concentration; pH-dependent analysis of NOR selectivity (PDF)

## ■ AUTHOR INFORMATION


### Corresponding Author

**Kai S. Exner** − *University of Duisburg-Essen, Faculty of Chemistry, Theoretical Catalysis and Electrochemistry, Universitätsstraße 5, Essen 45141, Germany; Cluster of Excellence RESOLV, Bochum 44801, Germany; Center for Nanointegration (CENIDE) Duisburg-Essen, Duisburg 47057, Germany;* orcid.org/0000-0003-2934-6075; Email: kai.exner@uni-due.de

### Authors

**Muhammad Usama** − *University of Duisburg-Essen, Faculty of Chemistry, Theoretical Catalysis and Electrochemistry, Universitätsstraße 5, Essen 45141, Germany*

**Samad Razzaq** − *University of Duisburg-Essen, Faculty of Chemistry, Theoretical Catalysis and Electrochemistry, Universitätsstraße 5, Essen 45141, Germany*

Complete contact information is available at: https://pubs.acs.org/10.1021/acsphyschemau.4c00058


### Author Contributions

‖M.U. and S.R. contributed equally to this work. CRediT: **Muhammad Usama** data curation, formal analysis, investigation, software, visualization, writing - review & editing; **Samad Razzaq** data curation, formal analysis, investigation, methodology, software, writing - review & editing; **Kai Steffen Exner** conceptualization, funding acquisition, project administration, supervision, writing - original draft, writing - review & editing.

### Notes

The authors declare no competing financial interest.

## ■ ACKNOWLEDGMENTS

M.U., S.R., and K.S.E. thank the Ministry of Culture and Science of the Federal State of North Rhine-Westphalia (NRW Return Grant) for financial support to carry out this study. K.S.E. additionally acknowledges funding by the Deutsche Forschungsgemeinschaft through the RESOLV Cluster of Excellence (EXC 2033-390677874 − RESOLV) as well as the research unit FOR 2982 "UNODE" [413163866]. M.U., S.R., and K.S.E. are thankful for fruitful discussions with Dr.

Ebrahim Tayyebi (University of Duisburg-Essen) and Maksim Sokolov (University of Duisburg-Essen) regarding the nitrogen oxidation reaction and the reported data-driven framework, respectively. In addition, M.U. and S.R. express their gratitude to Yousuf Mehmood for insightful discussions during the logic-building phase in the programming of this work.

## REFERENCES

(1) Erisman, J. W.; Sutton, M. A.; Galloway, J.; Klimont, Z.; Winiwarter, W. How a Century of Ammonia Synthesis Changed the World. *Nat. Geosci.* **2008**, *1* (10), 636−639.
(2) Chipoco Haro, D. A.; Barrera, L.; Iriawan, H.; Herzog, A.; Tian, N.; Medford, A. J.; Shao-Horn, Y.; Alamgir, F. M.; Hatzell, M. C. Electrocatalysts for Inorganic and Organic Waste Nitrogen Conversion. *ACS Catal.* **2024**, *14* (13), 9752−9775.
(3) Chen, J. G.; Crooks, R. M.; Seefeldt, L. C.; Bren, K. L.; Bullock, R. M.; Darensbourg, M. Y.; Holland, P. L.; Hoffman, B.; Janik, M. J.; Jones, A. K.; Kanatzidis, M. G.; King, P.; Lancaster, K. M.; Lymar, S. V.; Pfromm, P.; Schneider, W. F.; Schrock, R. R. Beyond Fossil Fuel−Driven Nitrogen Transformations. *Science* **2018**, *360* (6391), No. eaar6611.
(4) Smil, V. Global Population and the Nitrogen Cycle. *Sci. Am.* **1997**, *277* (1), 76−81.
(5) Wu, T.; Melander, M. M.; Honkala, K. Coadsorption of NRR and HER Intermediates Determines the Performance of Ru-$N_4$ toward Electrocatalytic $N_2$ Reduction. *ACS Catal.* **2022**, *12* (4), 2505−2512.
(6) Guo, C.; Ran, J.; Vasileff, A.; Qiao, S.-Z. Rational Design of Electrocatalysts and Photo(Electro)Catalysts for Nitrogen Reduction to Ammonia ($NH_3$) under Ambient Conditions. *Energy Environ. Sci.* **2018**, *11* (1), 45−56.
(7) Singh, A. R.; Rohr, B. A.; Schwalbe, J. A.; Cargnello, M.; Chan, K.; Jaramillo, T. F.; Chorkendorff, I.; Nørskov, J. K. Electrochemical Ammonia Synthesis—The Selectivity Challenge. *ACS Catal.* **2017**, *7* (1), 706−709.
(8) Genç, A. E.; Tranca, I. C. Adsorption Mechanism of the $N_2$ and NRR Intermediates on Oxygen Modified $MnN_4$ − Graphene Layers − a Single Atom Catalysis Perspective. *Phys. Chem. Chem. Phys.* **2023**, *25* (27), 18465−18480.
(9) Hu, Q.; Yang, K.; Peng, O.; Li, M.; Ma, L.; Huang, S.; Du, Y.; Xu, Z.-X.; Wang, Q.; Chen, Z.; Yang, M.; Loh, K. P. Ammonia Electrosynthesis from Nitrate Using a Ruthenium−Copper Cocatalyst System: A Full Concentration Range Study. *J. Am. Chem. Soc.* **2024**, *146* (1), 668−676.
(10) Ren, Y.; Yu, C.; Tan, X.; Huang, H.; Wei, Q.; Qiu, J. Strategies to Suppress Hydrogen Evolution for Highly Selective Electrocatalytic Nitrogen Reduction: Challenges and Perspectives. *Energy Environ. Sci.* **2021**, *14* (3), 1176−1193.
(11) Andersen, S. Z.; Čolić, V.; Yang, S.; Schwalbe, J. A.; Nielander, A. C.; McEnaney, J. M.; Enemark-Rasmussen, K.; Baker, J. G.; Singh, A. R.; Rohr, B. A.; Statt, M. J.; Blair, S. J.; Mezzavilla, S.; Kibsgaard, J.; Vesborg, P. C. K.; Cargnello, M.; Bent, S. F.; Jaramillo, T. F.; Stephens, I. E. L.; Nørskov, J. K.; Chorkendorff, I. A Rigorous Electrochemical Ammonia Synthesis Protocol with Quantitative Isotope Measurements. *Nature* **2019**, *570* (7762), 504−508.
(12) Anand, M.; Abraham, C. S.; Nørskov, J. K. Electrochemical Oxidation of Molecular Nitrogen to Nitric Acid − towards a Molecular Level Understanding of the Challenges. *Chem. Sci.* **2021**, *12* (18), 6442−6448.
(13) Xia, R.; Overa, S.; Jiao, F. Emerging Electrochemical Processes to Decarbonize the Chemical Industry. *JACS Au.* **2022**, *2* (5), 1054−1070.
(14) Iriawan, H.; Andersen, S. Z.; Zhang, X.; Comer, B. M.; Barrio, J.; Chen, P.; Medford, A. J.; Stephens, I. E. L.; Chorkendorff, I.; Shao-Horn, Y. Methods for Nitrogen Activation by Reduction and Oxidation. *Nat. Rev. Methods Primers* **2021**, *1* (1), 56.
(15) Tayyebi, E.; Exner, K. S. Refining Free-Energy Calculations for Electrochemical Reactions: Unveiling Corrections beyond Gas-Phase Errors for Solvated Species and Ions. *J. Phys. Chem. C* **2024**, *128* (33), 13732−13742.
(16) Wang, Y.; Yu, Y.; Jia, R.; Zhang, C.; Zhang, B. Electrochemical Synthesis of Nitric Acid from Air and Ammonia through Waste Utilization. *Natl. Sci. Rev.* **2019**, *6* (4), 730−738.
(17) Long, J.; Li, H.; Xiao, J. The Progresses in Electrochemical Reverse Artificial Nitrogen Cycle. *Curr. Opin. Electrochem.* **2023**, *37*, 101179.
(18) Dai, C.; Sun, Y.; Chen, G.; Fisher, A. C.; Xu, Z. J. Electrochemical Oxidation of Nitrogen towards Direct Nitrate Production on Spinel Oxides. *Angew. Chem. Int. Ed.* **2020**, *59* (24), 9418−9422.
(19) Kuang, M.; Wang, Y.; Fang, W.; Tan, H.; Chen, M.; Yao, J.; Liu, C.; Xu, J.; Zhou, K.; Yan, Q. Efficient Nitrate Synthesis via Ambient Nitrogen Oxidation with Ru-Doped $TiO_2$ /$RuO_2$ Electrocatalysts. *Adv. Mater.* **2020**, *32* (26), 2002189.
(20) Adalder, A.; Paul, S.; Ghorai, U. K. Progress of Electrochemical Synthesis of Nitric Acid: Catalyst Design, Mechanistic Insights, Protocol and Challenges. *J. Mater. Chem. A* **2023**, *11* (19), 10125−10148.
(21) Adalder, A.; Paul, S.; Ghorai, B.; Kapse, S.; Thapa, R.; Nagendra, A.; Ghorai, U. K. Selective Electrocatalytic Oxidation of Nitrogen to Nitric Acid Using Manganese Phthalocyanine. *ACS Appl. Mater. Interfaces* **2023**, *15* (29), 34642−34650.
(22) Karlsson, R. K. B.; Cornell, A. Selectivity between Oxygen and Chlorine Evolution in the Chlor-Alkali and Chlorate Processes. *Chem. Rev.* **2016**, *116* (5), 2982−3028.
(23) Fang, W.; Du, C.; Kuang, M.; Chen, M.; Huang, W.; Ren, H.; Xu, J.; Feldhoff, A.; Yan, Q. Boosting Efficient Ambient Nitrogen Oxidation by a Well-Dispersed Pd on MXene Electrocatalyst. *Chem. Commun.* **2020**, *56* (43), 5779−5782.
(24) Han, S.; Wang, C.; Wang, Y.; Yu, Y.; Zhang, B. Electrosynthesis of Nitrate via the Oxidation of Nitrogen on Tensile-Strained Palladium Porous Nanosheets. *Angew. Chem. Int. Ed.* **2021**, *60* (9), 4474−4478.
(25) Nørskov, J. K.; Rossmeisl, J.; Logadottir, A.; Lindqvist, L.; Kitchin, J. R.; Bligaard, T.; Jónsson, H. Origin of the Overpotential for Oxygen Reduction at a Fuel-Cell Cathode. *J. Phys. Chem. B* **2004**, *108* (46), 17886−17892.
(26) Hinnemann, B.; Moses, P. G.; Bonde, J.; Jørgensen, K. P.; Nielsen, J. H.; Horch, S.; Chorkendorff, I.; Nørskov, J. K. Biomimetic Hydrogen Evolution: $MoS_2$ Nanoparticles as Catalyst for Hydrogen Evolution. *J. Am. Chem. Soc.* **2005**, *127* (15), 5308−5309.
(27) Seitz, L. C.; Dickens, C. F.; Nishio, K.; Hikita, Y.; Montoya, J.; Doyle, A.; Kirk, C.; Vojvodic, A.; Hwang, H. Y.; Norskov, J. K.; Jaramillo, T. F. A Highly Active and Stable $IrO_x$ /$SrIrO_3$ Catalyst for the Oxygen Evolution Reaction. *Science* **2016**, *353* (6303), 1011−1014.
(28) Exner, K. S. Four Generations of Volcano Plots for the Oxygen Evolution Reaction: Beyond Proton-Coupled Electron Transfer Steps? *Acc. Chem. Res.* **2024**, *57* (9), 1336−1345.
(29) Isac, D. L.; Şoriga, Ş.-G.; Man, I.-C. How Do the Coadsorbates Affect the Oxygen Reduction Reaction Activity of Undoped and N-Doped Graphene Nanoribbon Edges? A Density Functional Theory Study. *J. Phys. Chem. C* **2020**, *124* (42), 23177−23189.
(30) Wan, H.; Bagger, A.; Rossmeisl, J. Limitations of Electrochemical Nitrogen Oxidation toward Nitrate. *J. Phys. Chem. Lett.* **2022**, *13* (38), 8928−8934.
(31) Tayyebi, E.; Höskuldsson, Á. B.; Wark, A.; Atrak, N.; Comer, B. M.; Medford, A. J.; Skúlason, E. Perspectives on the Competition between the Electrochemical Water and $N_2$ Oxidation on a $TiO_2$ (110) Electrode. *J. Phys. Chem. Lett.* **2022**, *13* (26), 6123−6129.
(32) Long, J.; Luan, D.; Fu, X.; Li, H.; Jing, H.; Xiao, J. Fundamental Insights on the Electrochemical Nitrogen Oxidation over Metal Oxides. *ACS Catal.* **2024**, *14* (7), 4423−4431.
(33) Olusegun, S. A.; Qi, Y.; Kani, N. C.; Singh, M. R.; Gauthier, J. A. Understanding Activity Trends in Electrochemical Dinitrogen Oxidation over Transition Metal Oxides. *ACS Catal.* **2024**, *14*, 16885−16896.


https://doi.org/10.1021/acsphyschemau.4c00058
*ACS Phys. Chem Au* 2025, 5, 38−46

(34) Huang, P.; Song, H.; Yoo, J.; Chipoco Haro, D. A.; Lee, H. M.; Medford, A. J.; Hatzell, M. C. Impact of Local Microenvironments on the Selectivity of Electrocatalytic Nitrate Reduction in a BPM-MEA System. *Adv. Energy Mater.* **2024**, *14* (28), 2304202.
(35) Shao, K.; Mesbah, A. A Study on the Role of Electric Field in Low-Temperature Plasma Catalytic Ammonia Synthesis via Integrated Density Functional Theory and Microkinetic Modeling. *JACS Au.* **2024**, *4* (2), 525−544.
(36) Ding, K.; Yang, T.; Leung, M. T.; Yang, K.; Cheng, H.; Zeng, M.; Li, B.; Yang, M. Recent Advances in the Data-Driven Development of Emerging Electrocatalysts. *Curr. Opin. Electrochem.* **2023**, *42*, 101404.
(37) Exner, K. S. A Universal Descriptor for the Screening of Electrode Materials for Multiple-Electron Processes: Beyond the Thermodynamic Overpotential. *ACS Catal.* **2020**, *10* (21), 12607−12617.
(38) Razzaq, S.; Exner, K. S. Materials Screening by the Descriptor $G_{max}(\eta)$: The Free-Energy Span Model in Electrocatalysis. *ACS Catal.* **2023**, *13* (3), 1740−1758.
(39) Exner, K. S. Beyond the Thermodynamic Volcano Picture in the Nitrogen Reduction Reaction over Transition-Metal Oxides: Implications for Materials Screening. *Chin. J. Catal.* **2022**, *43* (11), 2871−2880.
(40) Exner, K. S. Importance of the Walden Inversion for the Activity Volcano Plot of Oxygen Evolution. *Adv. Sci.* **2023**, *10* (36), 2305505.
(41) Exner, K. S. Steering Selectivity in the Four-Electron and Two-Electron Oxygen Reduction Reactions: On the Importance of the Volcano Slope. *ACS Phys. Chem. Au.* **2023**, *3* (2), 190−198.
(42) Exner, K. S. How Data-Driven Approaches Advance the Search for Materials Relevant to Energy Conversion and Storage. *Mater. Today Energy* **2023**, *36*, 101364.
(43) Rossmeisl, J.; Logadottir, A.; Nørskov, J. K. Electrolysis of Water on (Oxidized) Metal Surfaces. *Chem. Phys.* **2005**, *319* (1−3), 178−184.
(44) Exner, K. S. On the Mechanistic Complexity of Oxygen Evolution: Potential-Dependent Switching of the Mechanism at the Volcano Apex. *Mater. Horiz.* **2023**, *10* (6), 2086−2095.
(45) Man, I. C.; Su, H.; Calle-Vallejo, F.; Hansen, H. A.; Martínez, J. I.; Inoglu, N. G.; Kitchin, J.; Jaramillo, T. F.; Nørskov, J. K.; Rossmeisl, J. Universality in Oxygen Evolution Electrocatalysis on Oxide Surfaces. *ChemCatchem* **2011**, *3* (7), 1159−1165.
(46) Piqué, O.; Illas, F.; Calle-Vallejo, F. Designing Water Splitting Catalysts Using Rules of Thumb: Advantages, Dangers and Alternatives. *Phys. Chem. Chem. Phys.* **2020**, *22* (13), 6797−6803.
(47) Viswanathan, V.; Hansen, H. A. Unifying Solution and Surface Electrochemistry: Limitations and Opportunities in Surface Electrocatalysis. *Top. Catal.* **2014**, *57* (1−4), 215−221.
(48) Tao, H. B.; Zhang, J.; Chen, J.; Zhang, L.; Xu, Y.; Chen, J. G.; Liu, B. Revealing Energetics of Surface Oxygen Redox from Kinetic Fingerprint in Oxygen Electrocatalysis. *J. Am. Chem. Soc.* **2019**, *141* (35), 13803−13811.
(49) Cepitis, R.; Kongi, N.; Rossmeisl, J.; Ivaništšev, V. Surface Curvature Effect on Dual-Atom Site Oxygen Electrocatalysis. *ACS Energy Lett.* **2023**, *8* (3), 1330−1335.
(50) Abild-Pedersen, F. Computational Catalyst Screening: Scaling, Bond-Order and Catalysis. *Catal. Today* **2016**, *272*, 6−13.
(51) Divanis, S.; Kutlusoy, T.; Ingmer Boye, I. M.; Man, I. C.; Rossmeisl, J. Oxygen Evolution Reaction: A Perspective on a Decade of Atomic Scale Simulations. *Chem. Sci.* **2020**, *11* (11), 2943−2950.
(52) Sokolov, M.; Exner, K. S. Is the ∗O vs. ∗OH Scaling Relation Intercept More Relevant than the ∗OOH vs. ∗OH Intercept to Capture Trends in the Oxygen Evolution Reaction? *Chem. Catal.* **2024**, *4* (7), 101039.
(53) Man, I.-C.; Tranca, I. Derived Trends of the Oxygen Adsorption Energy Using the Simplistic Model of the Thermodynamic Potential for Oxygen Evolution Reaction. *Catal. Today* **2025**, *443*, 114963.
(54) Cepitis, R.; Ivaništšev, V.; Rossmeisl, J.; Kongi, N. Bypassing the Scaling Relations in Oxygen Electrocatalysis with Geometry-Adaptive Catalysts. *Catal. Sci. Technol.* **2024**, *14* (8), 2105−2113.
(55) Man, I.-C.; Tranca, I. Trends in the Oxygen Adsorption Energy Derived from the Thermodynamic Potential Model for the Oxygen Evolution Reaction. *Catal. Today* **2025**, *443*, 114963.
(56) Sargeant, E.; Illas, F.; Rodríguez, P.; Calle-Vallejo, F. Importance of the Gas-Phase Error Correction for O2 When Using DFT to Model the Oxygen Reduction and Evolution Reactions. *J. Electroanal. Chem.* **2021**, *896*, 115178.
(57) Urrego-Ortiz, R.; Builes, S.; Illas, F.; Calle-Vallejo, F. Gas-Phase Errors in Computational Electrocatalysis: A Review. *EES Catal* **2024**, *2* (1), 157−179.
(58) Nørskov, J. K.; Bligaard, T.; Rossmeisl, J.; Christensen, C. H. Towards the Computational Design of Solid Catalysts. *Nat. Chem.* **2009**, *1* (1), 37−46.
(59) Van Der Heijden, O.; Park, S.; Vos, R. E.; Eggebeen, J. J. J.; Koper, M. T. M. Tafel Slope Plot as a Tool to Analyze Electrocatalytic Reactions. *ACS Energy Lett* **2024**, *9* (4), 1871−1879.
(60) Exner, K. S. Controlling Stability and Selectivity in the Competing Chlorine and Oxygen Evolution Reaction over Transition Metal Oxide Electrodes. *ChemElectrochem* **2019**, *6* (13), 3401−3409.
(61) Rabiee, H.; Ge, L.; Zhang, X.; Hu, S.; Li, M.; Yuan, Z. Gas Diffusion Electrodes (GDEs) for Electrochemical Reduction of Carbon Dioxide, Carbon Monoxide, and Dinitrogen to Value-Added Products: A Review. *Energy Environ. Sci.* **2021**, *14* (4), 1959−2008.
(62) Kwon, S.; Stoerzinger, K. A.; Rao, R.; Qiao, L.; Goddard, W. A.; Shao-Horn, Y. Facet-Dependent Oxygen Evolution Reaction Activity of $IrO_2$ from Quantum Mechanics and Experiments. *J. Am. Chem. Soc.* **2024**, *146* (17), 11719−11725.
(63) Zaffran, J.; Stevens, M. B.; Trang, C. D. M.; Nagli, M.; Shehadeh, M.; Boettcher, S. W.; Caspary Toroker, M. Influence of Electrolyte Cations on Ni(Fe)OOH Catalyzed Oxygen Evolution Reaction. *Chem. Mater.* **2017**, *29* (11), 4761−4767.
(64) Huang, P.-W.; Tian, N.; Rajh, T.; Liu, Y.-H.; Innocenti, G.; Sievers, C.; Medford, A. J.; Hatzell, M. C. Formation of Carbon-Induced Nitrogen-Centered Radicals on Titanium Dioxide under Illumination. *JACS Au.* **2023**, *3* (12), 3283−3289.
(65) Steinmann, S. N.; Wang, Q.; Seh, Z. W. How Machine Learning Can Accelerate Electrocatalysis Discovery and Optimization. *Mater. Horiz.* **2023**, *10* (2), 393−406.
(66) Mistry, A.; Franco, A. A.; Cooper, S. J.; Roberts, S. A.; Viswanathan, V. How Machine Learning Will Revolutionize Electrochemical Sciences. *ACS Energy Lett.* **2021**, 1422−1431.

## NOTE ADDED AFTER ASAP PUBLICATION

This paper was published ASAP on December 24, 2024 with errors in equations 23 and 33. The corrected version was reposted on December 26, 2024.


https://doi.org/10.1021/acsphyschemau.4c00058
*ACS Phys. Chem Au* 2025, 5, 38−46